Research

CEG-0598, a novel dual inhibitor of EGFR and C5aR demonstrates in vitro anticancer and antimetastatic activity in prostate cancer cells

Ayed A. Dera[1] ⓘ · Majed Al Fayi[1] ⓘ

Abstract

Background The EGFR is abundantly expressed in prostate cancer (PC). The anaphylatoxin C5a induces leukocyte migration via the C5a receptor (C5aR) by releasing matrix metalloproteinases (MMP) to favor metastasis in the tumor microenvironment. This work aims to selectively inhibit the EGFR and C5aR in PC cells to abort cell growth/ proliferation and metastasis.

Methods For lead identification, high-throughput virtual screening (HTVS) of the ChemBridge library was followed by protein–ligand interaction profilers, GROMACS, and GMX-MMPBSA techniques. LNCaP and PC3 cells were used to validate in vitro efficacy.

Results HTVS identified CEG-0598 with favorable binding affinities of − 10.2 kcal/mol and − 13.5 kcal/mol towards EGFR and C5aR respectively. Molecular dynamic simulations demonstrated stable binding interactions for CEG-0598 with Root Mean Square Deviation values around 0.06 nm. The ΔG binding calculation was − 50.29, and − 51.64 for EGFR and C5aR respectively. ADME supported favorable small molecule characteristics and selective inhibition profiles. Kinome-wide off-target virtual screening predicted EGFR to have above-average docking scores. CEG-0598 inhibited EGFR and C5aR activities with IC_{50} values of 145.8 nM and 55.51 nM respectively. The compound effectively controlled the proliferation of LNCaP and PC3cells with GI_{50} values of 156.1 nM, and 112.2 nM respectively. CEG-0598 prompted dose-responsive apoptosis in the PC cells and decreased the tarns endothelial migration of both PC cells. Treatment with CEG-0598 reduced the C5a-induced MMP activity in the LNCaP and PC3cells.

Conclusion CEG-0598 is a selective EGFR/C5a dual inhibitor that downregulates MMP activity to control proliferation, migration and induce apoptosis, in PC cells warranting further preclinical developments.

Research Highlights

- The structure of EGFR, complexed with the ATP-competitive inhibitor AQ4, revealed a critical ATP-binding pocket for ligand interaction, highlighting key residues (e.g., ARG-310, GLY-304, TYR-300) involved in inhibitor binding.
- Virtual screening of the ChemBridge library against EGFR identified potential hit molecules with favorable binding affinities, which were further tested for dual targeting of EGFR and C5aR.
- CEG-598 emerged as a lead molecule after demonstrating strong binding affinities to both EGFR and C5aR, and favorable ADMET properties compared to other molecules in the screening process.

✉ Ayed A. Dera, ayedd@kku.edu.sa | [1]Department of Clinical Laboratory Sciences, College of Applied Medical Sciences, King Khalid University, Abha, Saudi Arabia.

- CEG-598 was found to stably bind to both EGFR and C5aR, with molecular dynamics simulations revealing minimal RMSD deviations and robust hydrogen bond formation, confirming its binding stability over 100 ns.
- CEG-598 inhibited EGFR and C5aR activities in enzyme assays and suppressed prostate cancer cell proliferation (LNCaP and PC3). It also induced apoptosis and blocked C5a-stimulated metastatic events, including endothelial migration and MMP8 activation.

1 Introduction

Prostate cancer remains one of the leading causes of cancer-related mortality in men worldwide, with tumor growth and metastasis posing significant challenges to effective treatment [1]. Metastasis, in particular, is the primary cause of prostate cancer-related deaths, as it allows cancer cells to invade distant organs [2]. Targeting these two pathways simultaneously offers a promising therapeutic strategy to combat both tumor growth and metastatic progression [3].

EGFR, a transmembrane tyrosine kinase receptor, is overexpressed in several cancers, including prostate cancer, where it drives cell proliferation, survival, and tumor progression. Activation of EGFR triggers downstream signaling cascades, such as the PI3K/AKT and MAPK pathways, which are pivotal for cellular growth and resistance to apoptosis [4]. Consequently, EGFR has become a prominent therapeutic target, with several inhibitors demonstrating success in clinical settings [5, 6]. However, while EGFR inhibition can effectively suppress tumor growth, it often fails to address metastatic potential, leaving a significant gap in comprehensive prostate cancer treatment [7, 8]. Addressing this gap requires a complementary approach to simultaneously target metastasis-driving pathways, such as the C5aR signaling axis, which regulates cancer cell migration and invasion [9].

The C5a-receptor (C5aR), a G protein-coupled receptor, plays a critical role in promoting metastasis in prostate cancer [10, 11]. Activation of C5aR by its ligand, C5a, initiates a cascade of events that enhance tumor cell motility, trans-endothelial migration, and extracellular matrix degradation [12, 13]. A key mediator in this pathway is MMP8, a matrix metalloproteinase responsible for degrading the extracellular matrix and facilitating cancer cell invasion into surrounding tissues [3, 14]. Elevated expression of MMP8 is strongly associated with poor prognosis in prostate cancer, underscoring its significance as a therapeutic target [15]. By inhibiting C5aR, it is possible to suppress MMP8 activity, thereby disrupting the metastatic cascade and limiting the spread of cancer cells.

Combining EGFR inhibition with C5aR-targeted therapy provides a novel dual-action approach to combat prostate cancer. While EGFR inhibition directly impacts tumor cell proliferation and induces apoptosis [16], C5aR inhibition complements this by blocking key metastatic mechanisms, including MMP8-mediated extracellular matrix degradation [3]. This integrated strategy not only addresses the primary tumor growth but also prevents metastatic dissemination, effectively tackling prostate cancer on multiple fronts. In this study, we explore the potential of dual inhibition of EGFR and C5aR to regulate MMP8 activity and disrupt the growth and mobility of prostate cancer cells, paving the way for innovative therapies against this aggressive disease. While previous studies have predominantly focused on either targeting EGFR to suppress tumor proliferation or inhibiting C5aR to prevent metastatic spread, there has been a significant gap in integrating these two strategies to achieve comprehensive cancer control. EGFR inhibitors such as Gefitinib and Erlotinib have shown efficacy in reducing tumor growth but often fall short in addressing metastatic potential [17, 18]. Conversely, C5aR inhibitors like PMX53 have demonstrated anti-metastatic properties by disrupting the C5a signaling axis, but they lack direct tumor-suppressive effects [19]. The lack of a unified therapeutic approach that simultaneously targets both proliferation and metastasis leave an unmet need, especially in aggressive cancers like prostate cancer. This study specifically addresses this critical gap by developing a dual-targeting strategy with CEG-598, a novel small molecule designed to inhibit both EGFR-mediated cell proliferation and C5aR-driven metastasis. By leveraging the dual inhibition potential of CEG-598, the study offers a promising therapeutic avenue that not only suppresses tumor growth but also effectively curtails the metastatic cascade, presenting a novel approach that has not been previously explored in prostate cancer therapy.

In this study, we focused on developing novel dual inhibitors targeting EGFR and C5aR to combat the growth and metastatic potential of prostate cancer cells. By leveraging computational screening, molecular docking, and dynamics simulations, we identified a compound that effectively binds to the ATP-binding pocket of EGFR and the protein–protein

interaction site of C5aR. Subsequent in vitro analyses validated the lead molecule's dual inhibitory action, demonstrating its potential as a therapeutic agent capable of suppressing both tumor proliferation and C5aR-mediated metastasis.

2 Materials and methods

2.1 Materials

All reagents, chemicals, buffers, standard compounds PMX53 (#219639-75-5), and Lapatinib (#231277-92-2) were obtained from Sigma Aldrich, USA. CEG-0598 (#5233147) was purchased from ChemBridge, San Diego, CA, USA. LNCaP, PC3, HUVEC, and Vero cells were from ATCC, USA. The C5aR inhibition kit (# BAH-C5AR1-C5-1) was from RayBiotech Life, Inc., GA, USA. EGFR Kinase Assay Kit (# 40321) was from BPS Bioscience San Diego, CA, USA. QCM™ Tumor Cell Trans-Endothelial Migration Assay kit (#ECM558) was from Merk Millipore, WI, USA. The Annexin V kit was from Thermo Scientific, MA, USA. PE Anti-MMP8 antibody [EP1252Y] (#ab211967) was from Abcam, MA, USA.

2.2 Methods

2.2.1 High-throughput virtual screening (HTVS)

A high-throughput virtual screening (HTVS) strategy was employed using the SiBioLEAD platform [20, 21] (https://sibiolead.com/) to identify potential dual inhibitors for EGFR and C5aR. The ChemBridge compound library, containing approximately 850,000 molecules, served as the source of screening compounds. The three-dimensional structures of EGFR (PDB ID: 4hjo) [22] and C5aR (PDB ID: 7y67) [23] were obtained from the Protein Data Bank (PDB) and prepared using standard protein preparation protocols. Initial filtering of the compound library was based on molecular weight (350–750 Da) and adherence to Lipinski's Rule of Five criteria to ensure drug-like properties. Docking studies were performed using Autodock Vina, integrated within the SiBioLEAD platform, to efficiently identify potential ligands targeting both EGFR and C5aR.

2.2.2 Molecular dynamics simulation (MDS)

Molecular dynamics (MD) simulations were employed to evaluate the stability and binding interactions of the top-ranked compounds through the HTVS. The GROMACS software suite, accessed via the SiBioLEAD MD simulation platform [24], was used for simulations. Protein–ligand complexes for EGFR and C5aR were immersed in a solvated triclinic box containing Simple Point Charge (SPC) water molecules. The system was parameterized using the OPLS force field, and sodium chloride (NaCl) was added at a physiological concentration of 0.15 M to neutralize the system. The simulation systems underwent energy minimization using the steepest descent algorithm to eliminate steric clashes and optimize geometry. This was followed by a two-phase equilibration process, lasting 300 ps under isothermal-isobaric conditions, to stabilize the systems before production runs. Production simulations were conducted for 100 ns, and trajectory data were analyzed for parameters such as Root Mean Square Deviation (RMSD) to assess the conformational stability of the protein–ligand complexes. Additionally, hydrogen bond and hydrophobic interaction analyses were performed to evaluate the consistency and strength of binding.

2.2.3 Gibbs free energy calculations

The binding free energies of the top-performing compounds were calculated using the Molecular Mechanics Poisson-Boltzmann Surface Area (MM-PBSA) method. Fifty representative frames were extracted from the 100 ns MD simulation trajectories of the EGFR::CEG-598 and C5aR::CEG-598 complexes. The gmx_MMPBSA tool, accessible via the SiBioLEAD platform [25], was used to compute binding free energy values, which included contributions from van der Waals forces, electrostatics, polar solvation, and non-polar solvation terms. Average binding free energies were calculated to assess the ligands' binding affinities to the target proteins. Compounds with the most negative free energy values were prioritized for further analysis.

2.2.4 ADMET profiling and kinome-wide virtual screening

The absorption, distribution, metabolism, excretion, and toxicity (ADMET) profiles of the shortlisted compounds were analyzed using the ADMET-AI tool available at https://admet.ai.greenstonebio.com/. Ligands were converted into Simplified Molecular Input Line Entry System (SMILES) format and uploaded to the platform for analysis. The tool generated detailed predictions for pharmacokinetic and toxicological properties, including absorption efficiency, metabolic stability, tissue distribution, and potential toxicity. Results were presented in graphical formats for easy comparison and selection of compounds with favorable drug-like characteristics. This step ensured that only compounds with optimal ADMET profiles were considered for further experimental validation.

For kinome-wide virtual screening, we used an automated algorithm from SiBioLEAD LLC which was previously explained [26]. Briefly, for this analysis, a library of protein kinases (310) which includes a broad range of kinases representing different kinase families is assembled. The selected compound is docked into the active sites of these kinases using the molecular docking method from Autodock-Vina. This predicts the binding affinity and poses of the compound in each kinase's active site.

2.2.5 EGFR kinase inhibition assay

The assay was performed using the EGFR Kinase Assay Kit per the manufacturer's instructions. Briefly, 25 µl/well of the master mix [that contains 6 µl of $5 \times$ kinase assay buffer, 1 µl of 500 µM ATP, 1 µl of PTK substrate (10 mg/ml), and 17 µl of distilled water] was added to the 96 well plates. This was followed by the addition of 5 µl of the Log dilutions (ranging from 0.1 nM to 10,000 nM) of CEG-0598 or the standard Lapatinib at the destinated final concentrations to the test wells, while the blank and positive control received 5 µl of diluent solution. The reaction was initiated by adding 20 µl of EGFR (1 ng/µl) prepared in $1 \times$ assay buffer to the test and positive control wells. Blank wells were added with 20 µl of $1 \times$ kinase buffer. The plate was incubated at 30 °C for 45 min. Following, 50 µl of Kinase-Glo Max reagent was added to each well, covered with aluminium foil, and incubated at room temperature for 15 min. The plate was read for luminescence using a FLUOstar Omega microplate reader (BMG LABTECH, NC, CARY, USA). Blank values were subtracted and the percentage inhibition of kinase activity was calculated and analyzed using GraphPad Prism software (version 6.0). Half-dose inhibitory concentration (IC_{50} values) was presented.

2.2.6 C5aR inhibition assay

Per the manufacturer's instruction, the assay was performed using a RayBio Custom Binding Assay Kit. Briefly, 100 µl Log dilutions (ranging from 0.1 nM to 10,000 nM) of CEG-0598 or the standard PMX53 mixed with ligand protein concentrate at the destinated final concentrations were added to the test wells pre-coated with Ca5R. The blank wells received 100 µl of diluent solution. The plate was incubated for 2.5 h at room temperature. Following this incubation, the wells were washed 4 times with $1 \times$ wash buffer and 100 µl of 1X detection antibody was added to all wells and incubated for 1 h at room temperature. This was followed by the 4 washes with $1 \times$ wash buffer and the addition of 1X HRP-Conjugated Anti-IgG solution to each well and incubated for 1 h. After 4 washed with $1 \times$ wash buffer, 100 µl TMB One-Step Substrate Reagent was then added to each well and incubated for another 30 min. The color formation was arrested by adding 50 µl stop solution directly to each well and read for absorbance at 450 nm using a FLUOstar Omega microplate reader (BMG LABTECH, NC, CARY, USA). Blank values were subtracted and the percentage inhibition of kinase activity was calculated and analyzed using GraphPad Prism software (version 6.0). Half-dose inhibitory concentration ($IC_{50)}$ values) were presented.

2.2.7 Cell culture and proliferation assay

LNCaP, PC3, and Vero cells were cultured in RPMI-1640 media with 10% FBS, 100 U/ml of penicillin, and 100 U/ml of streptomycin. The MTT assay was used to access proliferation as described elsewhere [27]. Briefly, the cells were seeded in 96 well plates (5×10^3 cells/well) and treated with Log dilutions (ranging from 0.1 nM to 10,000 nM) of CEG-0598 for 72 h. Followingly, the cells were added with 1 mg/ml MTT, incubated for 4h, and dissolved in DMSO. The contents were measured at 560 nm for absorbance. Percentage inhibition of cell proliferation was analyzed using the GraphPad Prism 6.0 software to determine the GI_{50} values.

2.2.8 Annexin V assay for apoptosis

The respective GI_{25}, GI_{50}, and GI_{100} doses of CEG-0598 for LNCaP and PC3 cells were tested for dose dependency in apoptosis assay. LNCaP cells were treated with 78 nM, 156 nM, and 312 nM of CEG-0598. Likewise, PC3 cells were treated with 56 nM, 112 nM, and 224 nM of CEG-0598. Both the PC cells were incubated for 48 h. Following the incubation period, the cells were washed using the kit's buffer, and stained for 15 min in the dark using 0.25 µg/ml Annexin V reagent. The cells were resuspended in a kit solution containing 0.5 µg/ml propidium iodide after two further washes. Flow cytometry was conducted by acquiring data from 10,000 events using a Guava easyCyte system, and the results were analyzed with InCyte software to distinguish between healthy and apoptotic cells (early and late phase apoptosis). The findings were presented using GraphPad Prism software (version 6.0; La Jolla, CA, USA).

2.2.9 C5a induced trans-endothelial migration assay

The assay was carried out using a calorimetry-based kit as per the manufacturer's instructions. Briefly, 1×10^5 of LNCaP or PC3 cells that were kept overnight in a serum-free media were added with 100 nM/L C5a and transferred to the inserts which were pre-grown with a monolayer of the HUVEC cells. LNCaP cells were treated with 78 nM, 156 nM, and 312 nM of CEG-0598. Likewise, PC3 cells were treated with 56 nM, 112 nM, and 224 nM of CEG-0598. The inserts were then transferred to new wells with cell growth media containing 50 ng/ml HGF. The PC cells now were allowed to migrate across the HUVEC membrane for 12 h in a CO_2 incubator. The inserts were removed from the wells, and stained for 15 min using the staining solution provided in the kit. Furthermore, the stain was eluted using the kit elution buffer and read for absorbance at 570 nm. Percentage inhibition of the cell migration across the HUVEC membrane was calculated concerning control and presented.

2.2.10 C5a induced MMP8 activity

MMP8 activity in the PC cells was analyzed by flow cytometry. LNCaP cells were exposed to 78 nM, 156 nM, and 312 nM of CEG-0598. Similarly, CEG-0598 at concentrations of 56 nM, 112 nM, and 224 nM was treated to the PC3 cells. Both the cell types were incubated for 60 min. Following this, both the cells were induced with 100 nM/L C5a for 4 h. Cell controls were set up for both PC cells. The cells were removed from the plates and transferred to sterile Eppendorf tubes. The cells were fixed with 4% formaldehyde for 10 min and then permeabilized with 90% methanol at $-20\,°C$ for 15 min. The cells were then incubated in $1 \times$ HBSS buffer/10% normal goat serum to block non-specific protein–protein interactions followed by the PE Anti-MMP8 antibody (1/500 dilution) for 30 min at $-20\,°C$. After two washes to remove the extra dye, the cells were suspended back in the HBSS buffer. Guava EasyCyte™ flow cytometer was used to acquire 5000 events. Analysis was carried out using InCyte software from Millipore, to enumerate the percentage positive populations of MMP8 in both cell types which were compared against the controls.

2.2.11 Statistical analysis

All experiments were performed in triplicate, and data were expressed as mean ± standard deviation (SD). Statistical analysis was conducted using GraphPad Prism software (version 6.0; La Jolla, CA, USA), and significance was determined using a two-tailed Student's t-test or one-way ANOVA, followed by post-hoc tests where applicable. A (*) p-value of <0.05 was considered statistically significant.

3 Results

3.1 Structure of EGFR identifies putative ligand binding site for novel lead molecules

To identify a dual inhibitor that targets both EGFR and C5A, we first targeted the EGFR structure. The three-dimensional structure of EGFR in a complex with the ATP-competitive inhibitor (4HJO) was retrieved from the PDB databank (Fig. 1a). Structure visualization highlights the ligand binding region (Fig. 1a). The ATP-binding pocket within the EGFR structure was identified, showing its critical role in ligand binding (Fig. 1b). Protein–ligand interaction profiling revealed interactions

Fig. 1 Structure of EGFR. **a** Three-dimensional representation of EGFR in complex with an ATP-competitive inhibitor (4HJO), colored based on secondary structure. **b** ATP-binding pocket in EGFR structure. **c** protein–ligand interaction profiling showing interactions of critical EGFR amino acid residues with known inhibitor (AQ4)
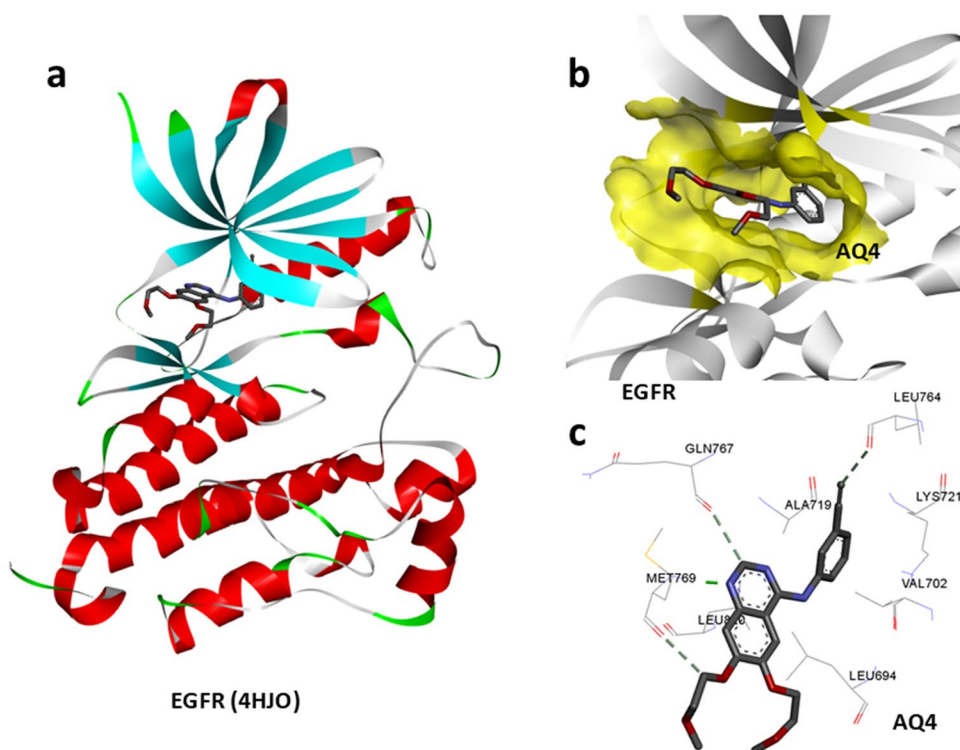
between key EGFR residues and the inhibitor AQ4, underscoring important amino acids involved in inhibitor binding (Fig. 1c).

3.2 High-throughput virtual screening of ChemBridge library identified hit molecules binding to EGFR

Toward identifying a novel dual inhibitor, we screened the ChemBridge library molecules (350–750 kDa) against EGFR. Docking scores predicted using the Diversity-based HTVS (D-HTVS) method against the EGFR kinase domain identified potential hit molecules with favorable binding affinities (Fig. 2a). To identify molecules binding to both EGFR and C5aR, we ought to screen the top hit-molecules identified from the EGFR screen against C5aR. For this, the cryo-electron microscopy structure of C5aR in complex with the Guanine-nucleotide binding protein was retrieved from the PDB databank, which provides a detailed visualization of the protein complex (Fig. 2b). Protein cavity prediction identified a druggable cavity at the protein–protein interface, indicating a potential site for therapeutic targeting (Fig. 2c).

3.3 C5aR docking and ADMET property calculations identified CEG-598 as lead molecule

Comparative analysis of docking scores for top molecules binding to both EGFR and C5aR demonstrated that CEG-598 exhibited strong binding affinities (Fig. 3a). We then calculated the ADMET properties for the top molecules showing binding affinities for both EGFR and C5aR, using ADMET-AI tool. Results show out of the top three molecules tested, CEG-598 possesses favorable drug-like properties compared to the other molecules (Fig. 3b), and therefore we pursued CEG-598 as our lead molecule for further studies.

3.4 Protein–ligand interaction analysis profiling shows CEG-598 targets critical amino acids in the EGFR kinase domain

Ligand binding pose analysis of CEG-598 with EGFR shows, the lead molecule binds at the ATP-binding pocket comfortably (Fig. 4a). Protein–ligand interaction analysis profiling of EGFR::CEG-598 complex shows, CEG-598 interaction with EGFR within the ATP-binding pocket of the kinase domain (Fig. 4b). The interaction analysis reveals that CEG-598 forms critical contacts with EGFR residues, including ARG-310, GLY-304, and TYR-300, within the ATP-binding pocket. Key interactions

Fig. 2 High-throughput virtual screening. **a** Predicted docking scores from the D-HTVS method against the EGFR kinase domain. **b** Three-dimensional representation of cryo-electro microscopy structure of C5A in complex with Guanine-nucleotide binding protein. **c** Protein cavity prediction showing the presence of a druggable cavity at the protein–protein interface
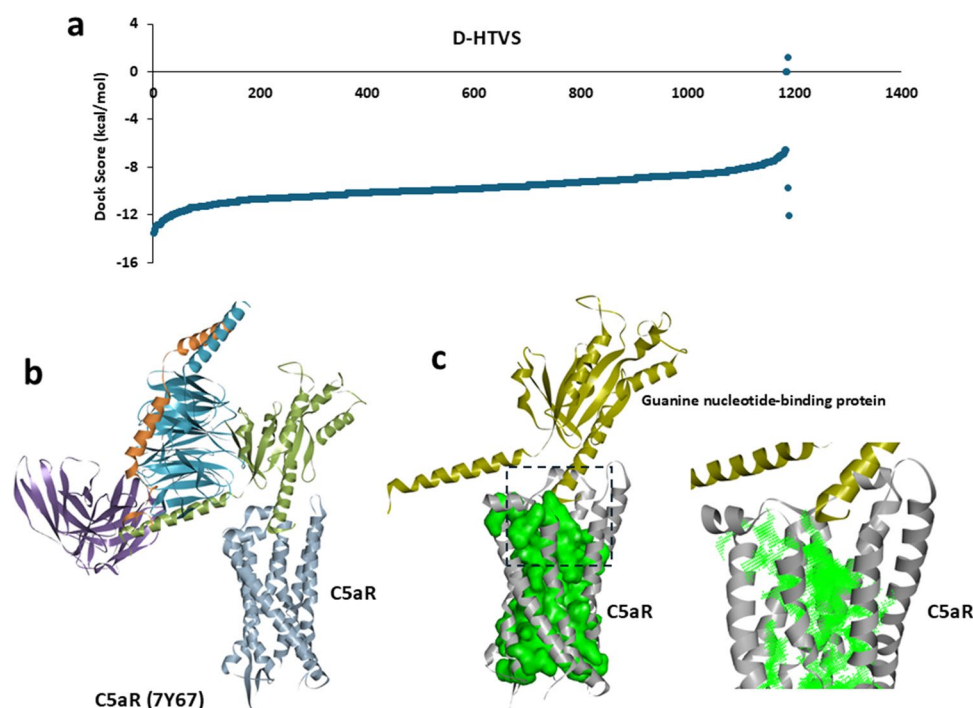
include hydrogen bonds and hydrophobic contacts, supporting stable ligand binding. Other residues such as ILE-299 and VAL-247 contribute through additional interactions, ensuring a well-fitted pose for the ligand (Fig. 4c).

Similarly, Ligand binding pose analysis of CEG-598 with C5aR also shows that the predicted lead molecule binds at the protein–protein interaction cavity of the C5aR protein (Fig. 4d). Protein–ligand interaction analysis profiling shows the lead molecules fit well within the cavity, which is indicative of a stable binding (Fig. 4e). Interaction analysis shows CEG-598 demonstrates several interactions with identified druggable cavities within C5aR. Key residues involved include ARG-817, ASP-831, and MET-769, forming a network of hydrogen bonds and hydrophobic interactions. Additional contacts with residues such as LEU-768, THR-834, and PRO-770 strengthen the binding pose, highlighting a favorable interaction profile for dual inhibition (Fig. 4f). Detailed table of hydrogen bonds and van der waals interactions were given in Supplementary Fig. 1a and b). Furthermore, in order to estimate the docking procedures, we performed docking analysis with known EGFR and C5a inhibitors, viz., lapatinib, and PMX53 respectively. Results show binding affinities for lapatinib and PMX53 towards EGFR and C5a respectively (Supplementary Figure c & d).

3.5 Molecular dynamics simulation of EGFR-CEG-598 complex shows CEG-598 binding stability

To investigate the dynamic binding stability of the identified lead molecule CEG-598 with EGFR, we performed an extensive molecular dynamics (MD) simulation under fully solvated conditions. The EGFR::CEG-598 complex was immersed in a triclinic box containing Simple Point Charge (SPC) water molecules and subjected to a 100 ns MD simulation. Snapshots of the simulation trajectories captured at 0 ns and 100 ns clearly demonstrated a stable interaction between CEG-598 and EGFR, with no noticeable changes in the binding conformation (Fig. 5a, b). This stability was further corroborated by analyzing the root mean square deviation (RMSD) of the ligand throughout the simulation period. The RMSD plot exhibited minimal deviation from the initial conformation, indicating that the ligand maintained a consistent binding pose within the ATP-binding pocket of EGFR throughout the 100 ns simulation (Fig. 5c). In addition to RMSD analysis, hydrogen bond profiling was conducted to assess the consistency of interactions between CEG-598 and EGFR. The hydrogen bond analysis revealed a stable pattern of interactions between key residues in the ATP-binding pocket and CEG-598, with hydrogen bonds consistently maintained throughout the entire simulation (Fig. 5d). This result highlights the robust interaction between CEG-598 and EGFR, which remained stable even during long-term dynamic conditions.

Similarly, to verify the binding stability of CEG-598 with C5A, a separate MD simulation was carried out under identical conditions, simulating the C5A::CEG-598 complex for 100 ns. Snapshots of the simulation trajectories captured at the start (0 ns) and the end (100 ns) of the simulation demonstrated that CEG-598 maintained a
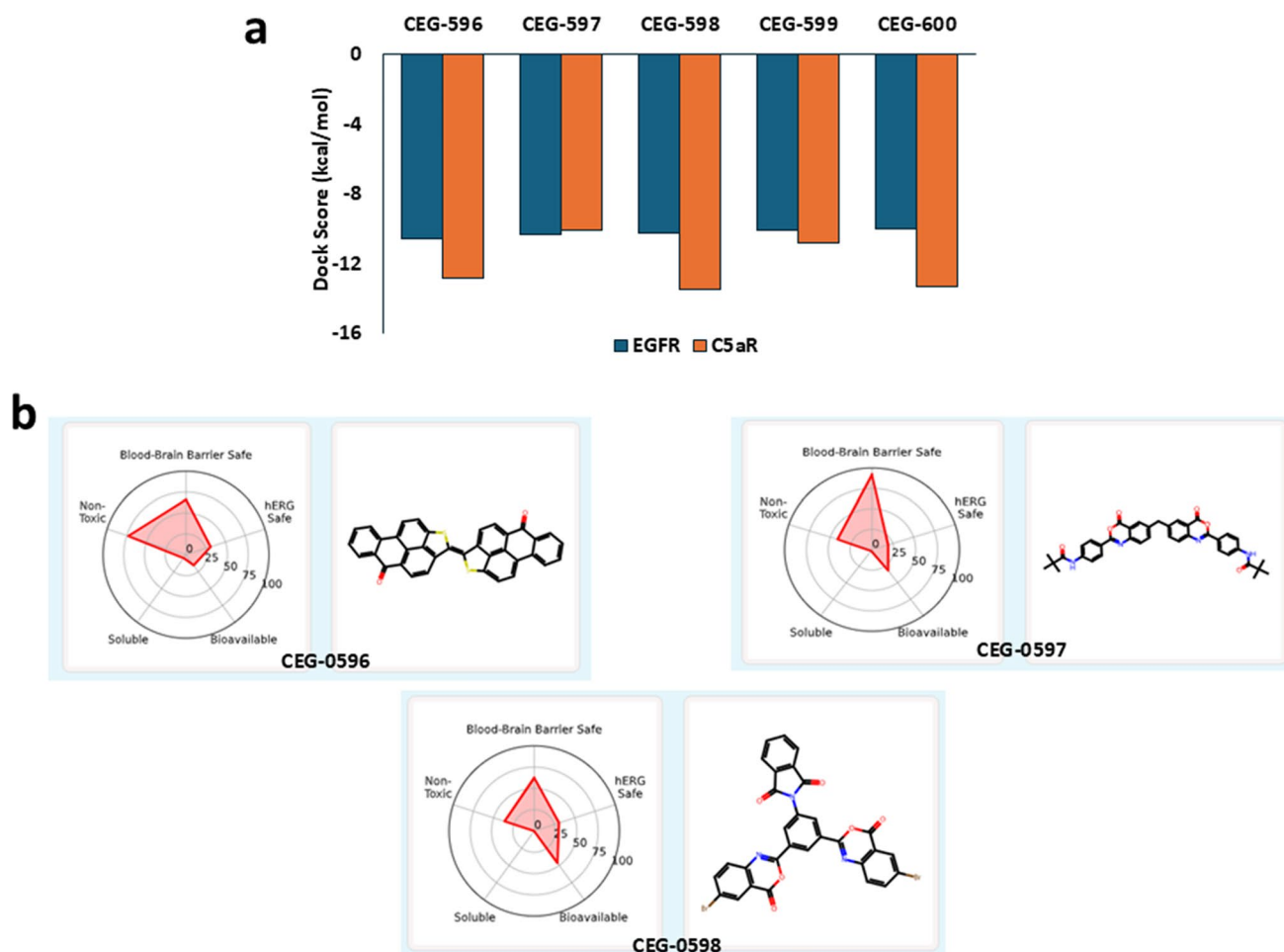
Fig. 3 ADMET property calculation predicts CEG-598 as a lead molecule. **a** Comparison of docking scores of top hit molecules between EGFR and C5A. **b** predicted ADMET properties of top-hit molecules binding to both EGFR and C5A

stable binding pose within the protein–protein interaction cavity of C5A (Fig. 6a, b). The RMSD analysis of CEG-598 during the simulation showed minimal fluctuations, indicating that the binding conformation remained consistent throughout the 100 ns simulation (Fig. 6c). Hydrogen bond analysis of the C5A::CEG-598 complex also confirmed the stability of interactions throughout the simulation period. Key hydrogen bonds between CEG-598 and critical residues in the C5A cavity were maintained over the entire trajectory, suggesting that the ligand remained tightly bound to the protein without any significant loss of interaction stability (Fig. 6d). These findings collectively demonstrate that CEG-598 exhibits strong and stable binding to both EGFR and C5A, as evidenced by consistent RMSD profiles and persistent hydrogen bond interactions over the duration of the simulations.

3.6 Gibbs binding free energy and kinome-wide virtual screening of CEG-598

Toward confirming the binding stability of CEG-598 with the proposed target proteins, viz., EGFR and C5aR, apart from docking scores, we calculated MMPBSA-based Gibbs binding energy estimates. Results indicated a favorable binding energy for CEG-598 with both EGFR, −50.29, (Fig. 7a) and C5aR, −51.64 (Fig. 7b). Furthermore, we performed a kinome-wide virtual screening for CEG-598 to see where EGFR stands in terms of overall kinome-wide. For this, 310 kinases were searched for their putative binding to CEG-598. Results highlighted the specific binding potential of CEG-598 with EGFR across the kinome, reinforcing its broad target specificity (Fig. 7c).
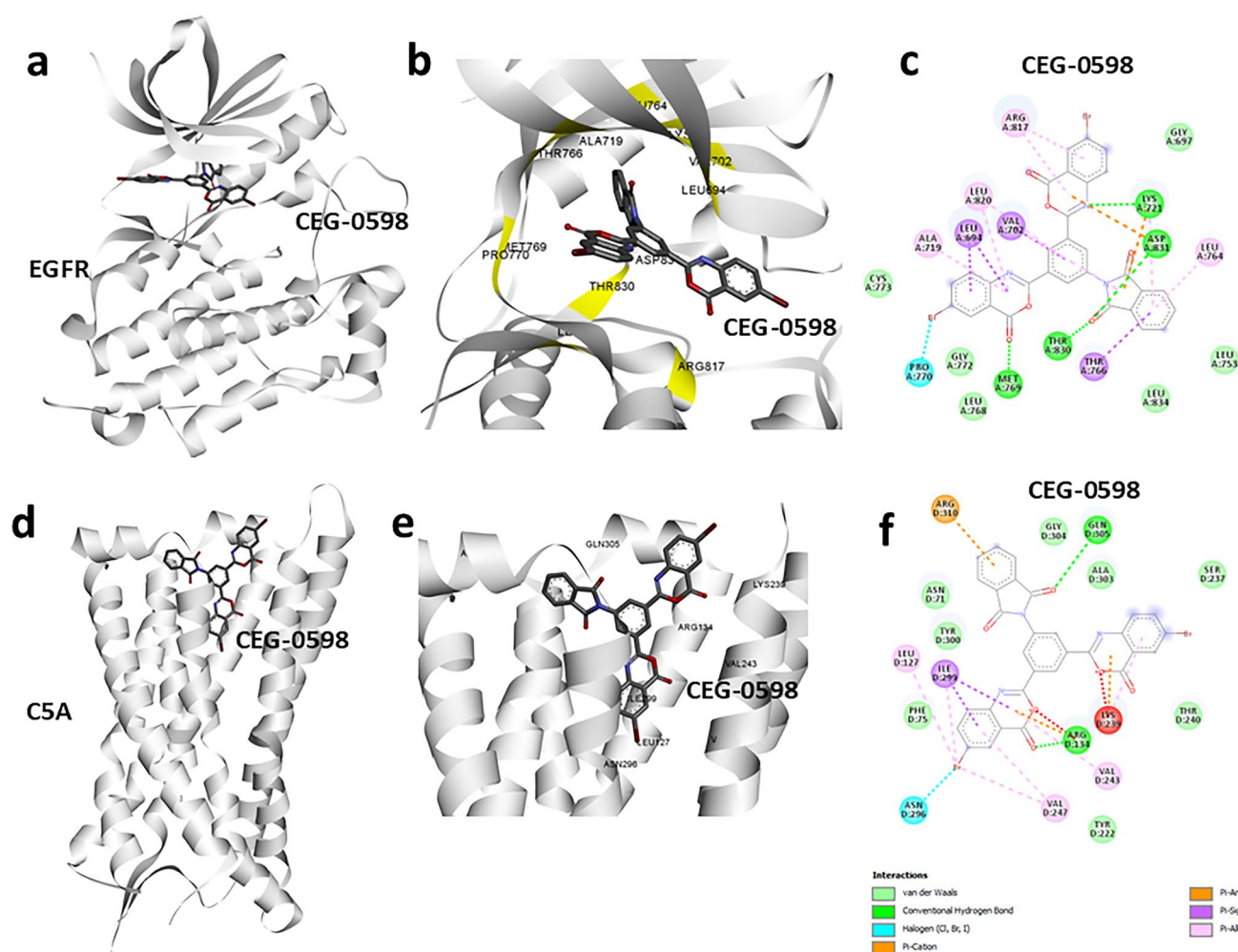
Fig. 4 Protein–ligand interaction profiling. **a** Protein–ligand interaction analysis showing the predicted dual inhibitor, CEG-598, binding to EGFR at the kinase domain. **b** 3D representation showing CEG-598 fits well within the ATP-binding pocket of the kinase domain. **c** 2D plot depicting the interactions of CEG-598 with EGFR. **d** Protein–ligand interaction analysis of CEG-598 bound to C5A. **e** 3D representation of CEG-598 binding pose with C5A. **f** 2D representation of amino acid residues of C5A interactions to CEG-598

3.7 CEG-0598 dually inhibited EGFR and C5aR to controlled PC cell proliferation

To check the translation of the computational prediction, we evaluated the inhibitory effect of CEG-0598 in cell-free enzyme-based assays. CEG-0598 effectively inhibited the EGFR kinase activity with an IC_{50} value of 145.8 nM (Fig. 8a). The standard EGFR inhibitor lapatinib showed an IC_{50} value of 10.26 nM (Fig. 8b). CEG-0598 inhibited the C5aR activity with an IC_{50} value of 55.51 nM (Fig. 8c). The standard C5aR inhibitor PMX53 showed an IC_{50} value of 24.70 nM (Fig. 8d).

Next, the efficacy of CEG-0598 to inhibit the proliferation of PC cells was evaluated. The compound inhibited the proliferation of both LNCaP and PC3 cell lines with respective GI_{50} values of 156.1 nM and 112.2 nM (Fig. 9a, b). The effect of the compound on normal Vero cells was evaluated. CEG-0598 inhibited Vero cell proliferation from 5000 nM and higher concentration (Fig. 9c).

3.8 CEG-0598 induced apoptosis and inhibited the C5a-stimulated metastatic events in PC cells

Treatment with CEG-0598 enhanced the number of early and late-phase apoptotic cells in PC cell types, eventually increasing total apoptosis (Fig. 10a). CEG-0598 treatment at 78 nM, 156 nM, and 312 nM raised total apoptosis to $32.0 \pm 5.77\%$, $43.40 \pm 4.70\%$, and $56.77 \pm 5.84\%$ in LNCaP cells respectively, while the control exhibited $3.60 \pm 1.26\%$

Fig. 5 Molecular Dynamic Simulation of EGFR bound to CEG-598. **a**, **b** Snapshot of trajectory frames taken at different time points (0, and 100 ns) showing the between EGFR and CEG-598. **c** Ligand RMSD calculated from 100ns simulation of CEG-598 bound to EGFR, showing a stable ligand RMSD plot. **d** Protein–ligand h-bond analysis calculated from 100 ns trajectory frames showing a stable interaction of CEG-598 with EGFR
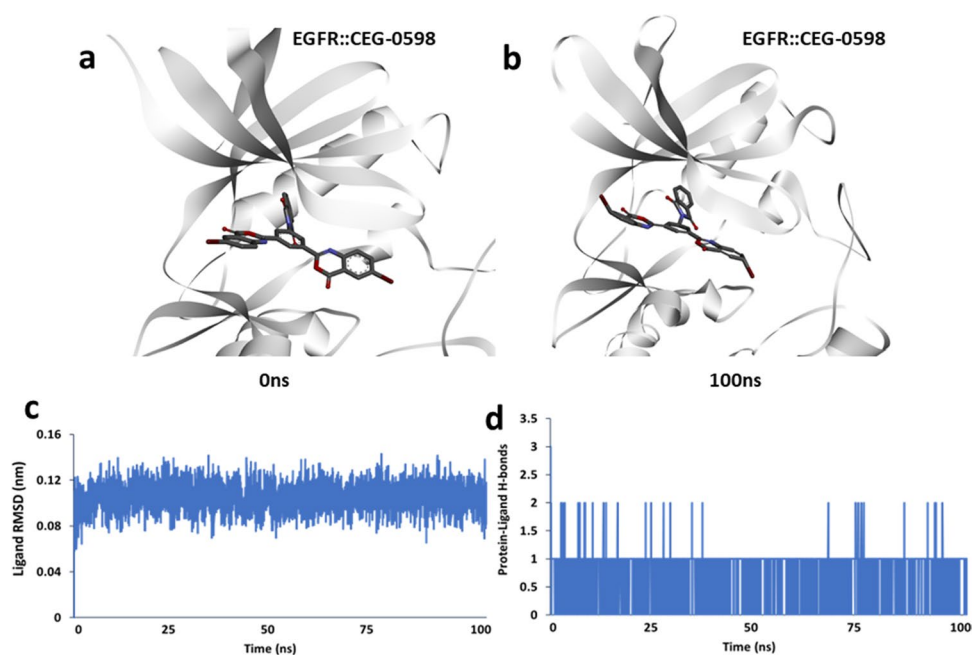

Fig. 6 Molecular dynamic simulation of C5A bound to CEG-598. **a**, **b** Snapshot of trajectory frames taken at different time points (0, and 100 ns) showing the between C5A and CEG-598. **c** Ligand RMSD calculated from 100 ns simulation of CEG-598 bound to C5A. **d** Protein–ligand h-bond analysis calculated from 100 ns trajectory frames showing a stable interaction of CEG-598 with EGFR
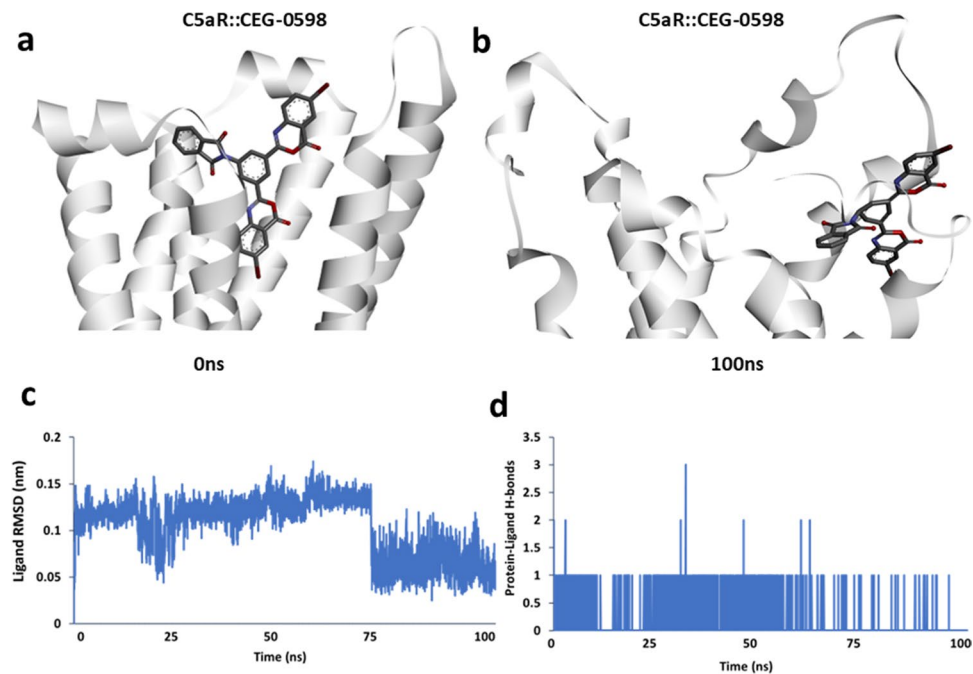
of total apoptotic populations (Fig. 10a). Similarly, CEG-0598 treatment at 56 nM, 112 nM, and 224 nM raised total apoptosis to $24.73 \pm 4.55\%$, $38.20 \pm 6.97\%$, and $49.46 \pm 6.05\%$ in PC3 cells respectively, while the corresponding control cells exhibited $5.90 \pm 2.40\%$ of total apoptotic populations (Fig. 10a).

Next, the antimetastatic efficacy of CEG-0598 in PC cells was tested by C5a-induced trans-endothelial cell migration assay. CEG-0598 dose dependently inhibited the endothelial trans-migration of LNCaP and PC3 cells across the HUVEC cell membrane under the influence of C5a (Fig. 10b).

Fig. 7 Gibbs binding free energy estimation and kinome-wide virtual screening. **a** Histogram showing calculated MMPBSA-based Gibbs binding free energy estimation of EGFR and CEG-598. **b** MMPBSA-based Gibbs binding free energy estimation for CEG-598 when bound to C5A. **c** Predicted docking scores for C5A with Kinome-wide virtual screening of all kinases
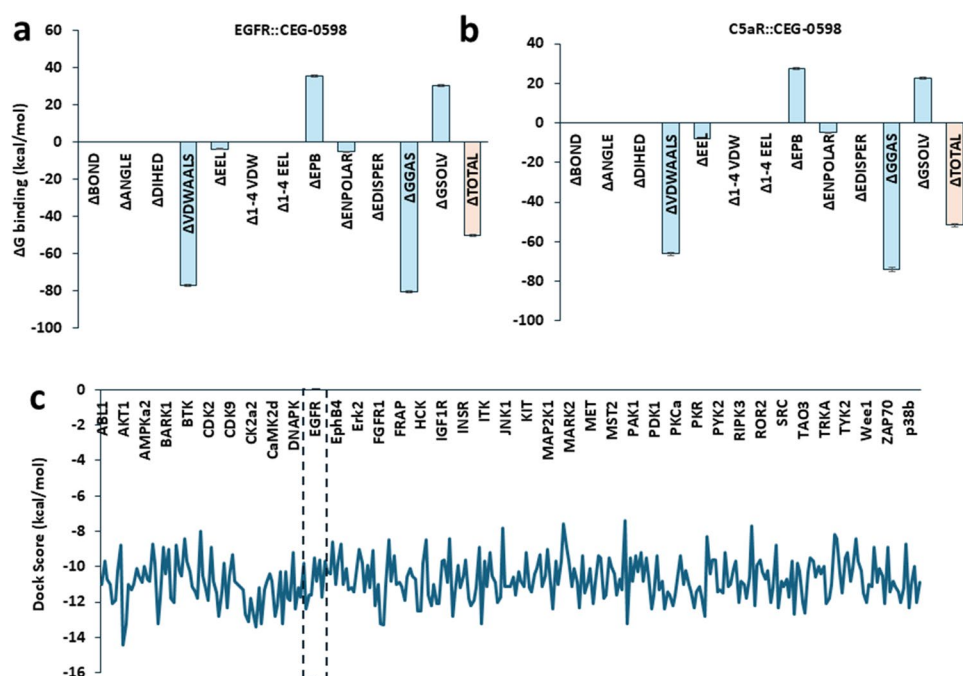

Fig. 8 Efficacy of CEG-0598 against dual kinase activities. Variable concentrations (0.1 nM to 10,000 nM) of the compound were tested against the activities of EGFR and C5aR were tested and the IC_{50} values were determined. **a** IC_{50} of CEG-0598 or **b** the standard compound lapatinib to inhibit the EGFR activity. **c** C_{50} of CEG-0598 or **d** the standard compound PMX53 to inhibit the Ca5R activity. Results expressed as mean ± SD from three experiments were analyzed using GraphPad Prism version 6.0 software
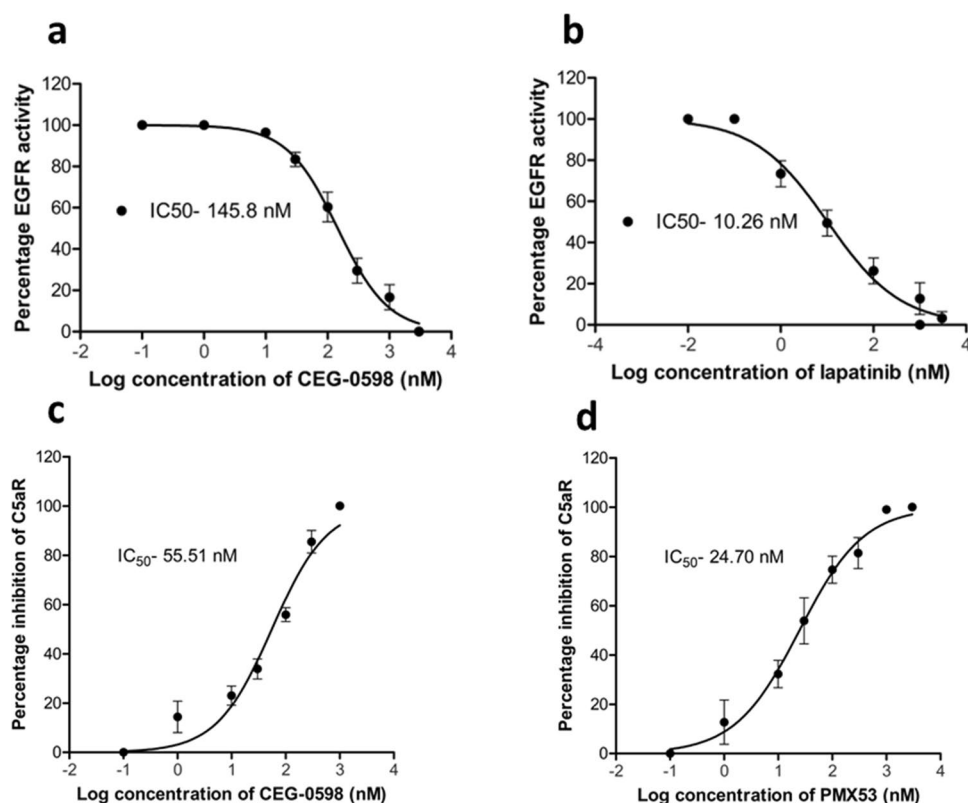
3.9 CEG-0598 decreased C5a stimulated MMP8 in LNCaP and PC3 cells

We next checked if the anti-metastatic efficacy of the compound was mediated by MMP activation. C5a-stimulated MMP8 expressions in PC cells were evaluated using flow cytometry. In the LNCaP cells, C5a stimulated MMP8 positive
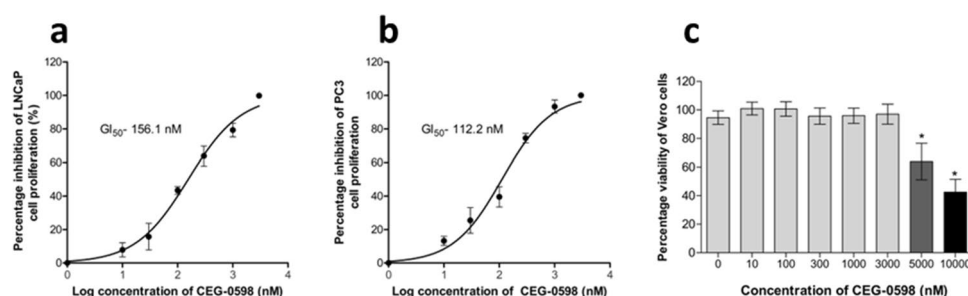
Fig. 9 Anti-proliferative effects of CEG-0598 in PC cells. The GI_{50} values of antiproliferative activity for **a** LNCap and **b** PC3 cells with CEG-0598 treatment are presented. **c** Effect of CEG-0598 concentrations on the viability of non-cancerous Vero cells. The MTT assay was used to assess cell proliferation and viability and mean±SD values of percentage proliferation inhibition or cell viability were analyzed using GraphPad Prism version 6.0 software
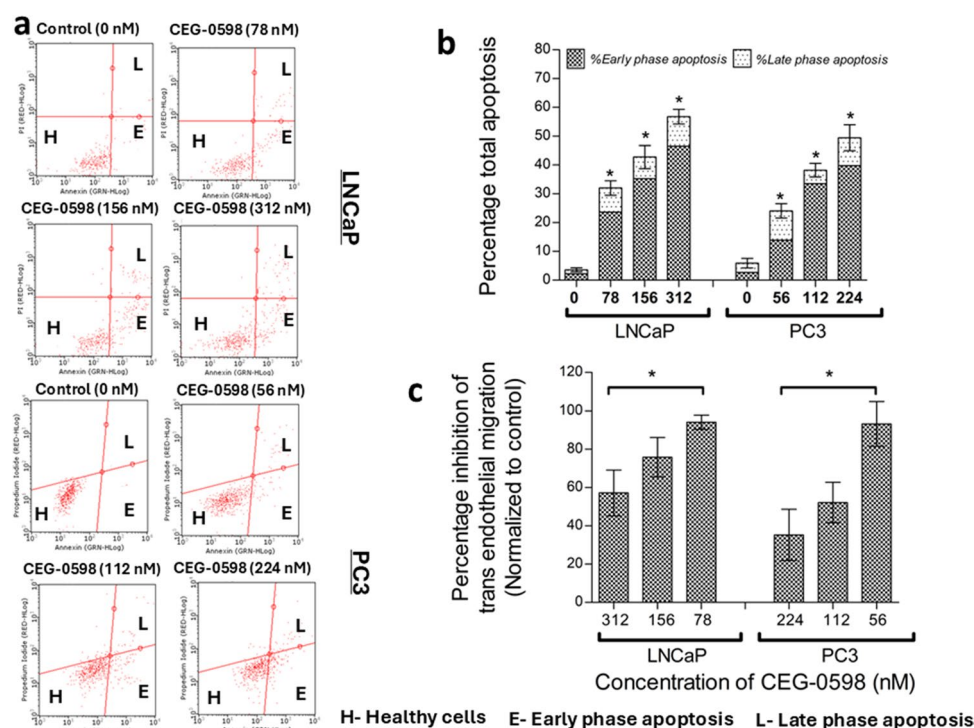

Fig. 10 Efficacy of CEG-0598 to promote apoptosis and inhibit C5a-mediated trans-endothelial migration in PC cells. **a** At 48 h of treatment, the CEG-0598 promoted early and late-phase apoptosis in both LNCaP and PC3 cells. All tests were conducted three times, and representative plots were provided. **b** Enumeration of early and late phase apoptosis levels in LNCaP and PC3 cells with CEG—598 treatments. The results are expressed as mean±SD and are statistically significant at *$p < 0.05$. **c** CEG-0598 dose dependently decreased the migration of LNCaP and PC3 cells across the HUVEC membrane under C5a influence. All tests were conducted three times, and representative results were provided. The results are expressed as mean±SD and statistically significant at *$p < 0.05$

population was found to be 57.01±7.11% (Fig. 11). Treatment with 78 nM, 156 nM, and 312 nM CEG-0598 reduced the MMP8 positive populations to 37.91±4.97%, 21.95±5.83%, and 9.37±4.10% respectively (Fig. 11). PC3 cells exhibited 69.88±6.38% MMP8 positive population when stimulated with C5a (Fig. 11). Treatment with 56 nM, 112 nM, and 224 nM of CEG-0598 reduced the MMP8 positive populations to 54.00±5.77%, 36.09±6.73% and 14.42±4.23% respectively in these cells (Fig. 11).
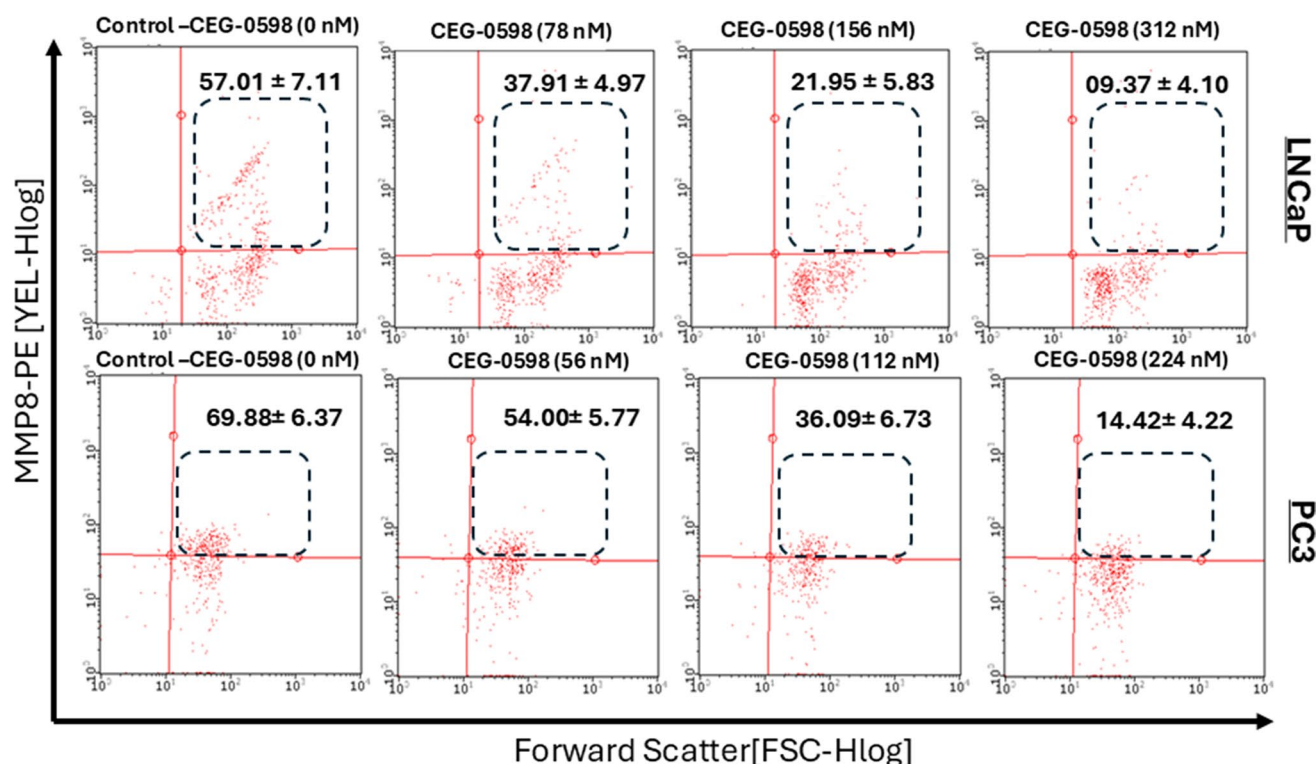
Fig. 11 MMP8 signaling was influenced by CEG-0598 treatment. Flow cytometric enumeration of MMP8 signaling with CEG-0598 in LNCaP and PC3 cells when induced with 100 nM/L C5a for 4 h. CEG-0598 downregulated MMP8-positive populations of these cells in a dose-dependent manner. Representative graphs are depicted. Numerical data are the average from three individual experiments. Statistical significance at $p < 0.05$

4 Discussion

The pursuit of therapies that simultaneously target multiple cancer progression pathways has become an innovative approach in combating the disease. This study underscores the dual inhibitory capability of CEG-598, effectively targeting both EGFR-driven proliferation and C5aR-mediated metastasis in prostate cancer. CEG-598 demonstrates stable binding within the ATP-binding pocket of EGFR, a critical therapeutic site, showcasing its potential as a potent anti-cancer agent. By employing a dual inhibition strategy, CEG-598 achieves both direct cytotoxicity to cancer cells and disruption of metastatic mechanisms, offering a multifaceted approach to addressing prostate cancer.

EGFR inhibitors have been widely recognized for their role in inducing apoptosis and halting cancer cell proliferation [4, 28]. Our findings affirm that CEG-598 effectively triggers apoptosis in prostate cancer cells by targeting EGFR, resulting in a marked increase in early- and late-stage apoptotic populations. This apoptotic activity complements CEG-598's anti-metastatic properties, reinforcing its value as a dual-function agent against aggressive cancer types. Traditional EGFR-targeted therapies predominantly focus on tumor growth suppression but often fail to mitigate metastatic progression [29]. CEG-598 overcomes this limitation by concurrently inhibiting C5aR-mediated signaling pathways [30]. This dual mechanism not only suppresses cellular proliferation but also restricts the spread of cancer cells, reducing tumor burden and minimizing the formation of secondary metastatic sites [31, 32]. Since the metastatic progression in prostate cancer frequently involves C5aR activation, which drives cellular migration and invasion [33], CEG-598's ability to inhibit C5a-induced trans-endothelial migration represents a significant advancement in curbing metastasis of PC [34]. Additionally, the compound's capacity to suppress MMP8, a key enzyme in the metastatic pathway, highlights its potential in targeting the C5aR-mediated metastatic axis [35]. This dual action establishes CEG-598 as a promising therapeutic molecule that addresses critical gaps in existing prostate cancer treatments.

Computational techniques largely facilitated the identification of CEG-598 as a dual inhibitor of EGFR and C5aR [36]. Molecular docking and protein–ligand interaction studies revealed that CEG-598 binds with high specificity to key residues in the ATP-binding pocket of EGFR and the interaction cavity of C5aR [37]. Combined with ADMET

property assessments, these computational insights led to the selection of a lead compound with favorable drug-like characteristics [38]. This in silico groundwork was instrumental in guiding subsequent in vitro validations of the compound's anti-cancer potential.

Molecular dynamics (MD) simulations have become an essential tool in modern drug discovery, offering deep insights into the stability and interaction dynamics of protein–ligand complexes [39]. In our study, MD simulations demonstrated the stable binding of CEG-598 to both EGFR and C5aR over a 100 ns trajectory, highlighting its potential as a dual-target inhibitor. The minimal root mean square deviation (RMSD) fluctuations observed during the simulations confirmed the strong binding affinity and stability of CEG-598 within the binding pockets of both target proteins. This consistency in binding position, even under dynamic conditions, is crucial for effective therapeutic action, as it indicates prolonged inhibitory activity at physiological temperatures [40]. Such findings reinforce confidence in the dual-inhibitory potential of CEG-598, as stable interactions are necessary for sustained therapeutic efficacy. The application of MD simulations in successful drug discovery has been well-documented, with several FDA-approved drugs benefiting from this computational approach. For instance, Darunavir, an HIV-1 protease inhibitor, relied on MD simulations to confirm its stable interaction within the active site of the protease, ultimately leading to its approval and widespread use [41]. Similarly, in the development of EGFR inhibitors such as Gefitinib and Erlotinib, MD simulations played a critical role in validating stable binding to the ATP-binding pocket, accelerating their transition through preclinical and clinical stages [42]. Our study also demonstrated consistent hydrogen bonding and robust hydrophobic interactions between CEG-598 and both targets, enhancing stability and anchoring the ligand within the binding site. This comprehensive computational strategy not only validates the dual-targeting capability of CEG-598 but also exemplifies the utility of in silico approaches in expediting the drug discovery process, as demonstrated by the successful development of drugs like Imatinib and Dasatinib for BCR-ABL and Sunitinib for receptor tyrosine kinases.

The computational findings were validated by in vitro verification using enzyme assays. CEG-598 inhibited EGFR and C5aR activities. The EGFR and C5aR standard compound depicted IC50 with the values as reported earlier [43, 44]. A pivotal finding of this study is the dose-dependent reduction in C5a-induced MMP8 expression in prostate cancer cells. Since MMP8 is a key facilitator of extracellular matrix degradation and cancer cell invasion, its suppression by CEG-598 underscores the compound's potential to modulate the tumor microenvironment and prevent metastasis [45]. This dual targeting of intracellular signaling pathways and extracellular matrix modulation positions CEG-598 as a leading candidate in innovative anti-cancer drug development. The mechanistic link between C5aR inhibition and MMP8 reduction primarily involves the disruption of downstream signaling pathways activated by C5aR, a G protein-coupled receptor that binds to the anaphylatoxin C5a. Upon activation, C5aR triggers several signaling cascades, including the PI3K/AKT, MAPK/ERK, and NF-κB pathways, which collectively promote the expression of matrix metalloproteinases such as MMP8 [46, 47]. Experimental evidence from various studies supports that blocking C5aR signaling not only lowers MMP8 levels but also reduces cancer cell migration and invasion [12, 48], establishing a clear mechanistic link between C5aR inhibition and the mitigation of metastatic processes.

On the other hand, resistance to EGFR inhibitors is a common challenge, often arising from mutations or compensatory pathway activation (e.g., PI3K/AKT, MAPK) [49]. While CEG-598 shows dual inhibition of EGFR and C5aR, prolonged use may still lead to resistance. Future studies should explore combination therapies targeting downstream pathways or alternative kinases and identify biomarkers to predict resistance, ensuring sustained efficacy in prostate cancer management.

This study is the first to propose a dual inhibition strategy targeting EGFR and C5aR in prostate cancer. Further research on the detailed mechanistic pathways and downstream target evaluations were not performed, which are limitations to this study. However, this preliminary study, by addressing both cancer cell proliferation and metastasis through a single therapeutic molecule, CEG-598 represents a groundbreaking step toward comprehensive prostate cancer management. Further investigations into its in vivo efficacy and safety will provide critical insights into its viability as a dual-action therapeutic for advanced prostate cancer.

5 Conclusion

In conclusion, this study presents a novel dual-targeting strategy to combat prostate cancer by selectively inhibiting EGFR and C5aR, two critical pathways involved in tumor proliferation and metastasis. The lead compound, CEG-598, demonstrates potent anti-cancer activity by stabilizing interactions within the ATP-binding pocket of EGFR and the C5aR protein–protein interaction cavity, effectively suppressing MMP8 expression and limiting metastatic spread.

Computational approaches, including virtual screening, molecular dynamics simulations, and free energy calculations, provided a robust foundation for identifying and validating the compound's dual-action capabilities. The integration of anti-proliferative and anti-metastatic effects highlights the therapeutic potential of CEG-598 as a promising candidate for advanced prostate cancer treatment, warranting further in vivo studies to confirm its efficacy and safety.

Declarations

Ethics approval, consent to participate, human and animal rights This article does not contain any studies with human participants or animals performed by any of the authors.

Consent for publication The authors give their consent to the journal for publication of this manuscript.

Competing interests The authors declare no competing interests.

References

1. Belkahla S, Nahvi I, Biswas S, Nahvi I, Ben Amor N. Advances and development of prostate cancer, treatment, and strategies: a systemic review. Front Cell Dev Biol. 2022;10: 991330.
2. Manna F, Karkampouna S, Zoni E, De Menna M, Hensel J, Thalmann GN, KruithofdeJulio M. Metastases in prostate cancer. Cold Spring Harbor Perspect Med. 2019;9: a033688.
3. Luchian I, Goriuc A, Sandu D, Covasa M. The role of matrix metalloproteinases (MMP-8, MMP-9, MMP-13) in periodontal and peri-implant pathological processes. Int J Mol Sci. 2022;23:1806.
4. Wee P, Wang Z. Epidermal growth factor receptor cell proliferation signaling pathways. Cancers. 2017;9:52.
5. Yamaoka T, Ohba M, Ohmori T. Molecular-targeted therapies for epidermal growth factor receptor and its resistance mechanisms. Int J Mol Sci. 2017;18:2420.
6. Wykosky J, Fenton T, Furnari F, Cavenee WK. Therapeutic targeting of epidermal growth factor receptor in human cancer: successes and limitations. Chin J Cancer. 2011;30:5–12.
7. Chang YS, Chen WY, Yin JJ, Sheppard-Tillman H, Huang J, Liu YN. EGF receptor promotes prostate cancer bone metastasis by downregulating miR-1 and activating TWIST1. Can Res. 2015;75:3077–86.
8. Lan H, Wu B, Jin K, Chen Y. Beyond boundaries: unraveling innovative approaches to combat bone-metastatic cancers. Front Endocrinol. 2023;14:1260491.
9. Gandaloviková A, Rosel D, Fernandes M, Veselý P, Heneberg P, Čermák V, Petruželka L, Kumar S, Sanz-Moreno V, Brábek J. Migrastatics-anti-metastatic and anti-invasion drugs: promises and challenges. Trends Cancer. 2017;3:391–406.
10. Imamura R, Kitagawa S, Kubo T, Irie A, Kariu T, Yoneda M, Kamba T, Imamura T. Prostate cancer C5a receptor expression and augmentation of cancer cell proliferation, invasion, and PD-L1 expression by C5a. Prostate. 2021;81:147–56.
11. Xu D, Li M, Ran L, Li X, Sun X, Yin T. C5aR1 promotes the progression of colorectal cancer by EMT and activating Wnt/β-catenin pathway. Clin Transl Oncol. 2023;25:440–6.
12. Darling VR, Hauke RJ, Tarantolo S, Agrawal DK. Immunological effects and therapeutic role of C5a in cancer. Expert Rev Clin Immunol. 2015;11:255–63.
13. Yoneda M, Imamura R, Nitta H, Taniguchi K, Saito F, Kikuchi K, Ogi H, Tanaka T, Katabuchi H, Nakayama H, Imamura T. Enhancement of cancer invasion and growth via the C5a–C5a receptor system: implications for cancer promotion by autoimmune diseases and association with cervical cancer invasion. Oncol Lett. 2019;17:913–20.
14. Kleiner DE, Stetler-Stevenson WG. Matrix metalloproteinases and metastasis. Cancer Chemother Pharmacol. 1999;43(Suppl):S42-51.

15. Escaff S, Fernández JM, González LO, Suárez A, González-Reyes S, González JM, Vizoso FJ. Study of matrix metalloproteinases and their inhibitors in prostate cancer. Br J Cancer. 2010;102:922–9.

16. Dutta PR, Maity A. Cellular responses to EGFR inhibitors and their relevance to cancer therapy. Cancer Lett. 2007;254:165–77.

17. Costa DB, Nguyen KS, Cho BC, Sequist LV, Jackman DM, Riely GJ, Yeap BY, Halmos B, Kim JH, Jänne PA, Huberman MS, Pao W, Tenen DG, Kobayashi S. Effects of erlotinib in EGFR mutated non-small cell lung cancers with resistance to gefitinib. Clin Can Res. 2008;14:7060–7.

18. Pao W, Chmielecki J. Rational, biologically based treatment of EGFR-mutant non-small-cell lung cancer. Nat Rev Cancer. 2010;10:760–74.

19. Luan X, Lei T, Fang J, Liu X, Fu H, Li Y, Chu W, Jiang P, Tong C, Qi H, Fu Y. Blockade of C5a receptor unleashes tumor-associated macrophage antitumor response and enhances CXCL9-dependent CD8(+) T cell activity. Mol Ther. 2024;32:469–89.

20. Alghamdi MA, Deshpande H. Dual targeting of MEK1 and Akt kinase identified SBL-027 as a promising lead candidate to control cell proliferations in gastric cancer. Biotechnol Appl Biochem. 2025. https://doi.org/10.1002/bab.2716.

21. Al Shahrani M, AboHassan M, Gahtani R, Alshahrani MY, Suliman M, Ahmad I, Saeed M. High-throughput screening and in vitro evaluation of CSB-0914; a novel small molecule NF-κB inhibitor attenuating inflammatory responses through NF-κB, Nrf2 and HO-1 cross-talk. J Biomol Struct Dyn. 2023;43:2771.

22. Park JH, Liu Y, Lemmon MA, Radhakrishnan R. Erlotinib binds both inactive and active conformations of the EGFR tyrosine kinase domain. Biochem J. 2012;448:417–23.

23. Feng Y, Zhao C, Deng Y, Wang H, Ma L, Liu S, Tian X, Wang B, Bin Y, Chen P, Yan W, Fu P, Shao Z. Mechanism of activation and biased signaling in complement receptor C5aR1. Cell Res. 2023;33:312–24.

24. Utami PD, Setianingsih H, Sari DRT. In silico approach triterpene glycoside of H. atra targeting orotidine 5-monophosphate decarboxylase protein (PfOMPDC) in P. falciparum infection mechanism. BioMed Res Int. 2024;2024: 5924799.

25. Rababi D, Nag A. A top-down approach for studying the in-silico effect of the novel phytocompound tribulusamide B on the inhibition of Nipah virus transmission through targeting fusion glycoprotein and matrix protein. Comput Biol Chem. 2024;112: 108135.

26. Abohassan M, Al Shahrani M, Ahmad I, Abullais SS, Srivastava S, Rajagopalan P. GC/MS characterization and computational kinome-wide screening of pomegranate fruit extract identifies key phytochemicals interacting to CDK kinases implicated in acute myeloid leukemia cells. J Food Biochem. 2022;46: e14178.

27. Abohassan M, Shahrani MMA, Alouda SK, Rajagopalan P. Dibenzo [a, c] phenazin-11-yl(phenyl) methanone (SBLJ23), a novel selective inhibitor targeting JAK2V617F mutation in myeloproliferative neoplasms. Oncol Res. 2025;33(3):675.

28. Wang M, Morsbach F, Sander D, Gheorghiu L, Nanda A, Benes C, Kriegs M, Krause M, Dikomey E, Baumann M, Dahm-Daphi J, Settleman J, Willers H. EGF receptor inhibition radiosensitizes NSCLC cells by inducing senescence in cells sustaining DNA double-strand breaks. Can Res. 2011;71:6261–9.

29. Hopper-Borge EA, Nasto RE, Ratushny V, Weiner LM, Golemis EA, Astsaturov I. Mechanisms of tumor resistance to EGFR-targeted therapies. Expert Opin Ther Targets. 2009;13:339–62.

30. Chen J, Li GQ, Zhang L, Tang M, Cao X, Xu GL, Wu YZ. Complement C5a/C5aR pathway potentiates the pathogenesis of gastric cancer by down-regulating p21 expression. Cancer Lett. 2018;412:30–6.

31. Feitelson MA, Arzumanyan A, Kulathinal RJ, Blain SW, Holcombe RF, Mahajna J, Marino M, Martinez-Chantar ML, Nawroth R, Sanchez-Garcia I, Sharma D, Saxena NK, Singh N, Vlachostergios PJ, Guo S, Honoki K, Fujii H, Georgakilas AG, Bilsland A, Amedei A, Niccolai E, Amin A, Ashraf SS, Boosani CS, Guha G, Ciriolo MR, Aquilano K, Chen S, Mohammed SI, Azmi AS, Bhakta D, Halicka D, Keith WN, Nowsheen S. Sustained proliferation in cancer: mechanisms and novel therapeutic targets. Semin Cancer Biol. 2015;35(Suppl):S25-s54.

32. Liu Z, Chen J, Ren Y, Liu S, Ba Y, Zuo A, Luo P, Cheng Q, Xu H, Han X. Multi-stage mechanisms of tumor metastasis and therapeutic strategies. Signal Transduct Target Ther. 2024;9:270.

33. Revel M, Daugan MV, Sautés-Fridman C, Fridman WH, Roumenina LT. Complement system: promoter or suppressor of cancer progression? Antibodies. 2020;9:57.

34. Kurihara R, Yamaoka K, Sawamukai N, Shimajiri S, Oshita K, Yukawa S, Tokunaga M, Iwata S, Saito K, Chiba K, Tanaka Y. C5a promotes migration, proliferation, and vessel formation in endothelial cells. Inflamm Res. 2010;59:659–66.

35. Gutiérrez-Fernández A, Fueyo A, Folgueras AR, Garabaya C, Pennington CJ, Pilgrim S, Edwards DR, Holliday DL, Jones JL, Span PN, Sweep FC, Puente XS, López-Otín C. Matrix metalloproteinase-8 functions as a metastasis suppressor through modulation of tumor cell adhesion and invasion. Can Res. 2008;68:2755–63.

36. Ward RA, Anderton MJ, Ashton S, Bethel PA, Box M, Butterworth S, Colclough N, Chorley CG, Chuaqui C, Cross DA, Dakin LA, Debreczeni J, Eberlein C, Finlay MR, Hill GB, Grist M, Klinowska TC, Lane C, Martin S, Orme JP, Smith P, Wang F, Waring MJ. Structure- and reactivity-based development of covalent inhibitors of the activating and gatekeeper mutant forms of the epidermal growth factor receptor (EGFR). J Med Chem. 2013;56:7025–48.

37. Sanders JM, Wampole ME, Thakur ML, Wickstrom E. Molecular determinants of epidermal growth factor binding: a molecular dynamics study. PLoS ONE. 2013;8: e54136.

38. Wu F, Zhou Y, Li L, Shen X, Chen G, Wang X, Liang X, Tan M, Huang Z. Computational approaches in preclinical studies on drug discovery and development. Front Chem. 2020;8:726.

39. Hollingsworth SA, Dror RO. Molecular dynamics simulation for all. Neuron. 2018;99:1129–43.

40. Otifi HM. SBL-JP-0004: a promising dual inhibitor of JAK2 and PI3KCD against gastric cancer. Oncol Res. 2025;33:235–43.

41. Ghosh AK, Dawson ZL, Mitsuya H. Darunavir, a conceptually new HIV-1 protease inhibitor for the treatment of drug-resistant HIV. Bioorg Med Chem. 2007;15:7576–80.

42. Amelia T, Kartasasmita RE, Ohwada T, Tjahjono DH. Structural insight and development of EGFR tyrosine kinase inhibitors. Molecules. 2022;27:819.

43. Konecny GE, Venkatesan N, Yang G, Dering J, Ginther C, Finn R, Rahmeh M, Fejzo MS, Toft D, Jiang SW, Slamon DJ, Podratz KC. Activity of lapatinib a novel HER2 and EGFR dual kinase inhibitor in human endometrial cancer cells. Br J Cancer. 2008;98:1076–84.

44. Kumar V, Lee JD, Clark RJ, Noakes PG, Taylor SM, Woodruff TM. Preclinical pharmacokinetics of complement C5a receptor antagonists PMX53 and PMX205 in mice. ACS Omega. 2020;5:2345–54.

45. Juurikka K, Butler GS, Salo T, Nyberg P, Åström P. The role of MMP8 in cancer: a systematic review. Int J Mol Sci. 2019;20:4506.

46. Luo S, Xu H, Gong X, Shen J, Chen X, Wu Z. The complement C3a–C3aR and C5a–C5aR pathways promote viability and inflammation of human retinal pigment epithelium cells by targeting NF-κB signaling. Exp Ther Med. 2022;24:493.

47. Steelman LS, Chappell WH, Abrams SL, Kempf RC, Long J, Laidler P, Mijatovic S, Maksimovic-Ivanic D, Stivala F, Mazzarino MC, Donia M, Fagone P, Malaponte G, Nicoletti F, Libra M, Milella M, Tafuri A, Bonati A, Bäsecke J, Cocco L, Evangelisti C, Martelli AM, Montalto G, Cervello M, McCubrey JA. Roles of the Raf/MEK/ERK and PI3K/PTEN/Akt/mTOR pathways in controlling growth and sensitivity to therapy-implications for cancer and aging. Aging. 2011;3:192–222.

48. Ajona D, Zandueta C, Corrales L, Moreno H, Pajares MJ, Ortiz-Espinosa S, Martínez-Terroba E, Perurena N, de Miguel FJ, Jantus-Lewintre E, Camps C, Vicent S, Agorreta J, Montuenga LM, Pio R, Lecanda F. Blockade of the complement C5a/C5aR1 axis impairs lung cancer bone metastasis by CXCL16-mediated effects. Am J Respir Crit Care Med. 2018;197:1164–76.

49. Koulouris A, Tsagkaris C, Corriero AC, Metro G, Mountzios G. Resistance to TKIs in EGFR-mutated non-small cell lung cancer: from mechanisms to new therapeutic strategies. Cancers. 2022;14:3337.

Discover